Applied Physics A (2020) 126:404
https://doi.org/10.1007/s00339-020-03538-x

Applied Physics A
Materials Science & Processing

S.I.: CURRENT STATE-OF-THE-ART IN LASER ABLATION

^{10}B-based films grown by pulsed laser deposition for neutron conversion applications

Maura Cesaria[1] · Antonella Lorusso[1,2] · Anna Paola Caricato[1,2] · Paolo Finocchiaro[3] · Simone Amaducci[3,4] · Maurizio Martino[1,2] · Muhammad Rizwan Aziz[1] · Lucio Calcagnile[2,5] · Alessio Perrone[1,2] · Gianluca Quarta[2,5]

Received: 9 October 2019 / Accepted: 9 April 2020 / Published online: 11 May 2020

Abstract
Solid-state neutron detectors exploit nuclear interactions producing energetic charged particles within a converter layer embedding nuclei with high neutron capture cross section and with thickness compatible with the charged particle range. Recently, boron-10 (^{10}B) is being considered as a valid alternative to the expensive and decreasingly available ^{3}He gas thanks to its large neutron absorption cross section and high-energy reaction products. Minimized amounts of impurities, films with optimal and well-controlled thickness, good uniformity over large areas and good adhesion to the substrates are essential to achieve efficient neutron detection performance. In this study, we present well-adherent 1-μm-thick ^{10}B-enriched boron coatings, deposited over a large area by off-axis pulsed laser deposition (PLD) using a nanosecond Nd-YAG laser beam operating at 1064 nm and high fluence (~ 10 J/cm^2), onto 1-mm-thick Al substrate as well as smooth and rough C substrates. By combining plasma plume divergence and peaked profile under off-axis deposition geometry, uniform ^{10}B films were obtained over an area of a 3.4 × 3.4 cm^2. We discuss the morphological characteristics of our deposits as related to the mechanisms of nanosecond laser ablation and present energy dispersive spectroscopy (EDS) elemental analysis of the film, paying attention to the different surface features. Negligible presence of O, N and C contaminants was achieved by controlled vacuum conditions. Moreover, we present encouraging neutron detection performances of our film deposited onto Al.

Keywords Solid neutron-to-charge converter · Boron coatings · Pulsed laser deposition · Boron enrichment · Textured substrate

1 Introduction

Early studies of boron (B) date back to two centuries ago and point out the ability of boron to combine with almost any element to form compounds [1]. The first report on pure boron in 1957 [2] documented a very complex structure which is nowadays known to have the most varied polymorphs (at least sixteen) including interlinked B_{12} icosahedra structural units arranged/linked in different lattice architectures [3, 4].

Boron and boron compounds have outstanding physical properties, such as high hardness (comparable to diamond), high stability of B–B bonds, corrosion resistance, low densities, high melting temperatures, high reflectance in the extreme ultraviolet (40–200 nm), as well as tunable thermal and electric transport properties depending on the dimensionality (thin films, nanowires, boron fullerene (B_{40} molecules), borophene (graphene-like structures composed of boron atoms) [5–8]. It results in a large number of application areas that make up the elemental boron and boron-based materials of scientific and technological interest. For instance, elemental boron films can be used in thermoelectric energy conversion devices operating at high temperatures [9], as protective coatings and biomedical implants

✉ Anna Paola Caricato
annapaola.caricato@unisalento.it

[1] Department of Mathematics and Physics "Ennio De Giorgi", University of Salento, Lecce, Italy

[2] National Institute of Nuclear Physics (INFN), Lecce, Italy

[3] National Institute of Nuclear Physics (INFN) - Laboratori Nazionali del Sud, Catania, Italy

[4] Department of Physics and Astronomy, University of Catania, Catania, Italy

[5] Centre of Applied Physics, Dating and Diagnostics (CEDAD), Department of Mathematics and Physics "Ennio De Giorgi", University of Salento, Lecce, Italy

[10, 11], for producing extreme UV optics [12], automotive parts [13] and neutron detectors [14, 15]. In particular, neutron detection has a broad range of applications in science, industry and medicine from life sciences, material investigation, radiation monitoring in nuclear power plants, nuclear material survey and homeland security [16, 17]. Due to their charge neutrality, the detection mechanism of thermal neutrons (0.0259 eV) relies on second-order effects, that is, production of charged particles, detectable by subsequent interaction–ionization processes, following capture reactions on neutron reactive nuclei. Since the worldwide availability of the most used converter element (^{3}He, mainly produced by the radioactive decay of tritium) [18] is strongly decreasing with the subsequently increasing cost [19], research and development (R&D) of neutron detection programs is actually aiming at replacing the technology based on ^{3}He gas [20]. In the field of large area neutron detectors, one possible solution to the ^{3}He shortage crisis is the replacement of ^{3}He by the boron isotope ^{10}B, which is one of the two stable isotopes of boron, taking advantage of its natural abundance of about $6x10^8$ times higher than that of ^{3}He [21], as well as its high neutron capture cross section (3842 barns) in $^{10}B(n,\alpha)^7Li$ reactions and quite large charged particles Q-values. To detail, the $^{10}B(n,\alpha)^7Li$ conversion reaction results in two main branching ratio (BR) channels leading to lithium and helium nuclei as ionizing products through the following reactions:

1. to ground state of ^{7}Li, BR ~ 6%: ^{7}Li (1.01 MeV) + α(1.78 MeV) with $Q = 2.79$ MeV,
2. to 1st excited state ^{7}Li, BR ~ 94%: ^{7}Li (0.84 MeV) + α(1.47 MeV) + γ(0.48 MeV) with $Q = 2.31$ MeV.

Boron-based neutron converter layers are preferentially inserted in solid-state neutron detectors because boron in gaseous form (BF_3) is toxic and favors detector aging. The working principle of semiconductor neutron detector is that α particles and Li ions generated within the neutron reactive layer following neutron-^{10}B reactions lose their energy while moving across a semiconductor diode-like architecture where they create electron–hole pairs that are in turn collected as an electrical signal. Since natural boron contains 20% of the neutron active ^{10}B isotope and 80% of the neutron inactive ^{11}B isotope, commercially available sources of boron are usually ^{10}B enriched to enhance the number of neutron converter interaction events.

For the alpha particles produced in $^{10}B(n,\alpha)^7Li$ reactions having short ranges (average ranges of 3.6 µm at 1.47 MeV (94% branching ratio) and 4.4 µm at 1.78 MeV (6% branching ratio)), micrometer-sized (one to several microns) boron coatings are usually optimized-thickness converters. Indeed, the boron-based converter layer is demanding to be thick enough to enable high-density production of α particles through absorption of most incident neutrons and thin enough to let efficient collection of sufficiently energetic α particles outside the converter layer, while taking into account charged particle energy loss in the layer. Moreover, B-based neutron detectors with efficient performance demand high-quality neutron converting films with minimum amount of unfavorable impurities (H, C, N and O), uniform thickness over large areas (to favor neutron capture and limit the energy dispersion of charged products), good adhesion to the substrates, as well as reduced aging effects and degradation under operational conditions.

In practice, producing adherent high-quality thick boron-based films is challenging because high melting point and lightweight of boron make difficult to evaporate and sputter, respectively, boron sources [22]. Moreover, adhesion problems to common substrates result from hardness-related high intrinsic stress buildup during deposition and, due to low thermal conductivity and brittle nature, boron targets can disintegrate under thermal loads.

Deposition of boron thin films is documented based on vacuum arc evaporation [10, 23], magnetron sputtering [24, 25], chemical vapor deposition (CVD) [26, 27], radio frequency (RF) [28] and microwave plasma-assisted CVD (PACVD) [26, 29–31], electron beam evaporation [32] and pulsed laser deposition (PLD) [33–37]. In general, CVD approaches use expensive, toxic and often explosive feed gases and require high growth temperature. Among physical vapor deposition (PVD) methods, PLD could be a promising choice to grow boron-based films thanks to its peculiar features (out of equilibrium nature, supersaturated deposition flux, hyperthermal regime, flexible interplay of the deposition parameters) that make it suitable to grow, onto various substrates, metastable phases and materials difficult or impossible to deposit commonly [38, 39].

In this paper, we present and discuss the results and preliminary achievements of our off-axis geometry PLD-based deposition of ^{10}B-enriched boron thick films onto various substrates (Si, Al, smooth and textured C substrates). In the case of Al substrates, we report on the successful deposition of 1-µm-thick adherent films with thickness profile nearly uniform over an area of a 3×3 cm^2 and discuss the morphological characteristics of the deposit as related to the mechanisms of laser ablation in the nanosecond-pulse regime. Moreover, we present detailed morphology and elemental composition analysis of boron deposits onto C substrates by comparing a smooth substrate with a textured one. In perspective of applications in the field of neutron detection, we also present preliminary encouraging achievements concerning the performance of our samples as thermal neutrons converter layers.

2 Experimental

2.1 PLD depositions

PLD depositions were performed by ablating a commercial 95% ^{10}B-enriched high-purity (99.9%) boron sintered target (about 45–55% in relative density, purchased from American Elements Company, USA). The schematics of a PLD experimental setup depicted in Fig. 1a also illustrate the dynamics of the PLD technique [38]. A pulsed laser beam striking a target of the material to be deposited induces, under proper focusing and delivered energy conditions, its removal (ablation). A so-called plasma plume forms, that is, a peaked highly forward-directed distribution of the species ejected from the target, that vehicles the transfer of the energetic ablated material from the target to the substrate surface where they deposit and rearrange driven by hyperthermal kinetics. In our experiments, a laser beam of the fundamental wavelength (1064 nm) of a Q-switched Continuum Powerlite-8010 Nd:YAG laser with pulse width of 7 ns was focused, by means of a focusing lens, and got to the boron target at an incidence angle of 45°. The boron target was placed within a stainless steel deposition chamber evacuated down to a base pressure of the order of 10^{-6} Pa by a combined (rotative plus turbomolecular) system of vacuum pumps. During laser irradiation, the boron bulk target was kept at room temperature and rotated with an angular speed of 1 Hz and contemporaneously spanned, to avoid cratering under multiple irradiation of the same area. The focusing area of the laser beam on the target was 8.8 mm^2, and experiments were performed with fluence value $F = \sim 10$ J/cm^2 [34] at a repetition rate of 10 Hz. A deposition rate of 0.28 Å/pulse was estimated, leading to a deposition run lasting 70 min for depositing 1-µm-thick boron film.

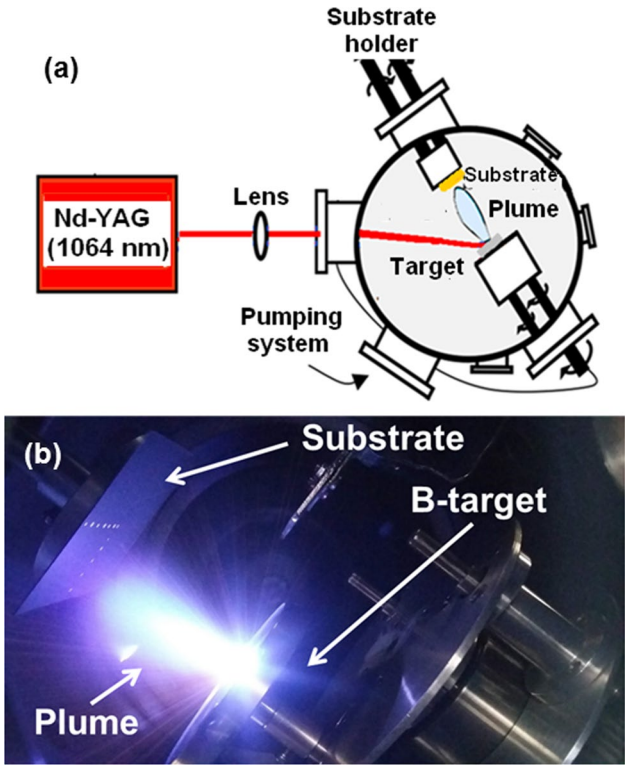

Fig. 1 **a** Schematics of the experimental setup and working principle of the PLD technique. **b** Picture of the performed PLD ablation experiment showing, as indicated by arrows, the boron target, the boron-containing plasma plume under off-axis geometry conditions and the collector substrate surface

Off-axis rather than conventional on-axis PLD deposition geometry was implemented to improve film uniformity over a large area [33, 40]. To detail, while in the case of on-axis configuration the plasma expansion axis corresponds to the center of the substrate, for the on-axis configuration the plasma expansion axis is shifted of about 1.4 cm from the center of the substrate (Fig. 1b).

Different substrates were considered, namely silicon (Si(100)), aluminum (Al) and carbon-fiber distributions, termed smooth and rough to refer to different surface texture/roughness, placed at a distance of 5 cm away from the boron target. Our preliminary experiments, performed by using the natural boron target mainly due to the high cost of ^{10}B-enriched material, yielded film detachment from the Si substrates for hundreds of nanometer-thick boron deposit. On the contrary, it was possible to deposit up to 4-µm-thick boron coatings onto 1-mm-thick Al substrates without observing delamination of the film and substrate distortion at room temperature deposition. Turning to the C substrates, the same experimental conditions as the ones used to deposit boron coatings onto Al substrates were set.

2.2 SEM and EDS analyses

The deposited boron coatings were inspected by scanning electron microscope (SEM) analysis using a JEOL-JSM-6480LV microscope. In addition, energy-dispersive X-Ray spectroscopy (EDS) microanalysis equipped with SEM was performed to study the elemental distribution in terms of the presence of B and contaminants (such as oxygen (O), carbon (C) and nitrogen (N)) in the deposits, paying attention to the presence of surface features stemming from the ablation mechanism.

EDS analysis was carried out by operating with an acceleration voltage of the electron beam of 2 kV. The electron beam was focused on selected points of a SEM image of the sample, and the collected X-ray signal was processed to obtain spectra with peaks associated with the atomic species within the deposits.

2.3 Neutron detection performances

A simple detector configuration was assembled in order to test the effectiveness of the ^{10}B-enriched boron layers produced by PLD as neutron converters. The sample was fixed on top of a silicon detector (30 mm × 30 mm × 0.3 mm) at 0.2 mm distance. This assembly was enclosed into a small iron box and placed inside a moderator, made from polyethylene blocks, along with a ^{252}Cf neutron source producing 8×10^3 neutrons/s (Fig. 2). The test, by irradiation of the detector setup with the moderated neutrons, consisted of two phases: (1) with the ^{10}B layer directly facing the silicon detector; (2) by reversing the sample so that the backing was facing the silicon diode thus preventing the produced particles from reaching the diode. By subtraction, one can then isolate the contribution of the neutron capture on the ^{10}B from all the other (background) contributions basically due to the large amount of gamma rays produced directly by the ^{252}Cf neutron source and by other neutron-induced reactions on the materials surrounding the detector.

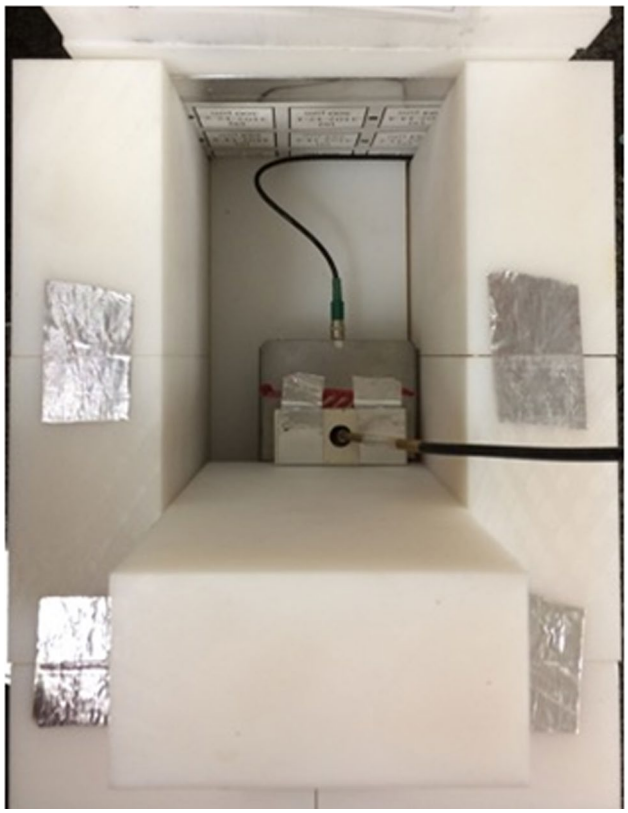

Fig. 2 Setup for neutron detection tests constituted by a moderator, made of polyethylene blocks, surrounding the detector box containing the ^{10}B neutron converter and the silicon diode (the moderator polyethylene top cover was removed to take the picture). The 252Cf neutron source, handled by means of the black stick shown on the right, is inserted into the circular housing visible on top of the detector box

3 Results and discussion

3.1 Morphology and elemental composition of the coatings

The general morphological characteristics of the 1-μm-thick boron coating deposited onto Al substrate are shown in Fig. 3, where different magnification levels enable to observe uniform morphology of the deposit and the occurrence of droplet-like surface features with wide size dispersion (from tens of nanometers to a few microns). The presence of such micro- and nanoaggregates may be accounted for the mechanisms of nanosecond laser ablation, that is, evaporation, boiling explosion and fragmentation by pressure recoil [41, 42] that account for deposition of a mixture of vapor species, droplets and irregular debris. Indeed, temperature and pressure gradients lead to deposition of irregular melted debris formed around the ablation crater (heat-affected zones), ejection of a large number of melt droplets from the target under explosive boiling conditions and formation of nanoclusters by gas-phase condensation in plasma plume [34]. For the laser wavelength used in our experiment (1064 nm), a depth of the crater in boron target of 3 μm per pulse was reported [34]. Because of low thermal diffusivity of boron material, the formation of craters deeper than the optical penetration depth (~ 1 μm), resulting from absorption coefficient of the order of 10^6 m^{-1} at 1064 nm, would indicate an additional mechanism concurring to mass removal together with explosive boiling. In this respect, it was proposed fragmentation due to a compressive wave, generated by recoil pressure at the target surface, that propagates underneath the target surface [42]. On this basis, the distribution of micrometer-sized spherical-like droplets exhibited by the boron deposit under consideration (Fig. 3) can be ascribed to explosive release of melt from the irradiated volume driven by the high-fluence regime set in our experiments [34]. In addition, the large surface features with irregular shape, particularly evident in Fig. 3c, would be debris resulting from fragmentation processes within the boron target. At least, condensation of the vapor species within the supersaturated volume of the plasma plume is responsible of the smaller spherical droplets dispersed in between the micrometer-sized droplets. By comparison with the literature [34], our sample exhibits reduced density and size of both micrometer droplets and irregular shaped clusters, which can be ascribed to different target-to-substrate distance and ablation spot area.

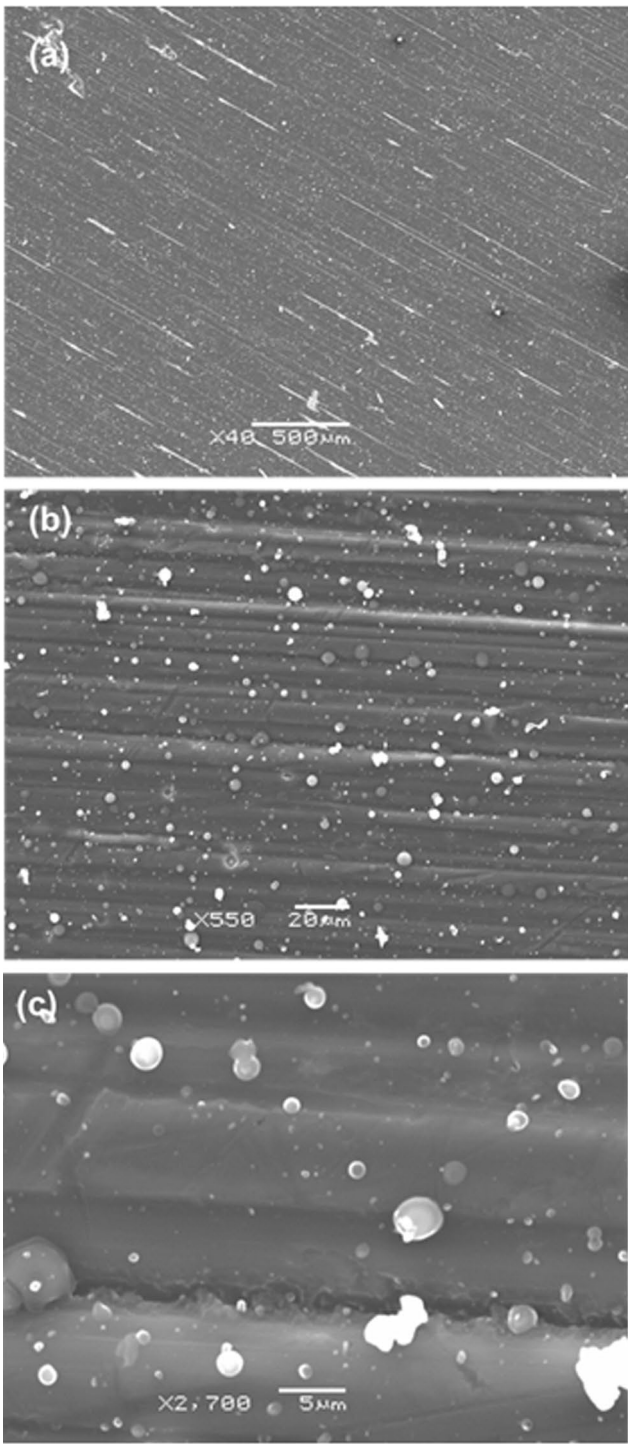

Fig. 3 SEM plan view micrographs, with progressively increasing magnification going from **a** to **c**, of the boron coating deposited onto 1-mm-thick Al substrate

In addition to morphology, thickness uniformity (Fig. 4) and elemental composition (Fig. 5) in terms of spatial distribution of boron and possible environmental contaminants were investigated.

Thickness uniformity tests were performed by a profilometer for an 1-µm-thick boron coating deposited onto a Si substrate under the same PLD conditions as the boron coating deposited onto 1-mm-thick Al substrate. Figure 4a shows the plot of the film thickness measured versus the distance from the center of the film along two perpendicular directions (labeled by positive and negative coordinates) including the measurement points reported in Fig. 4b. As a result of off-axis PLD deposition configuration, film thickness was found to be almost uniform over an area of 3.4×3.4 cm^2 (Fig. 4). The film thickness was estimated with an uncertainty of about 10%.

In regard to contaminants, some impurities may be incorporated in the growing film stemming from the boron target and environmental contamination, such as carbon (C), oxygen (O) and nitrogen (N). In particular, the content of O has to be minimized to limit neutron detection loss effects under thermal neutron irradiation.

The results of EDS elemental analysis of our 1-µm-thick boron coating deposited onto an Al substrate are shown in Fig. 5. Panel (a) provides a microscope image of the investigated area where the measurement points are indicated by a cross and labeled by a number (from 1 to 4). Panel (b) shows the boron signal measured over the different measurement points reported in panel (a). Noteworthy, the whole surface of the sampled area was analyzed to ascertain the presence of boron everywhere. Panel (c) reports on the EDS spectra corresponding to the measurement spots labeled in panel (a).

In particular, the B-Kα peak at 0.183 keV, the C-Kα peak at 0.277 keV, the N-Kα peak at 0.392 keV and the O-Kα peak at 0.525 keV are clearly indicated on the recorded EDS spectra.

According to the results of Fig. 5b, the smallest intensity of boron signal was found over the region surrounding the micrometer-sized cluster (Fig. 5a). This result is consistent with the size of the droplet in Fig. 5a being larger than the (average) film thickness and the droplet standing out of the film. Figure 5c shows scarcely visible O and N peaks, which is expected on the basis of the low background pressure achieved within the vacuum chamber before PLD depositions. In regard to C, its peak is clearly observable in the EDS spectra acquired at the measurement points 2 and 4, which are not associated with microdroplets. Accounting for the acceleration voltage (2 kV) of the electron beam set for the acquisition of the EDS spectra, processing of Al sheet is very likely to be responsible for the detected C signal. Indeed negligible C contribution was measured in the case of the measurement points 1 and 3 under the same EDS working conditions.

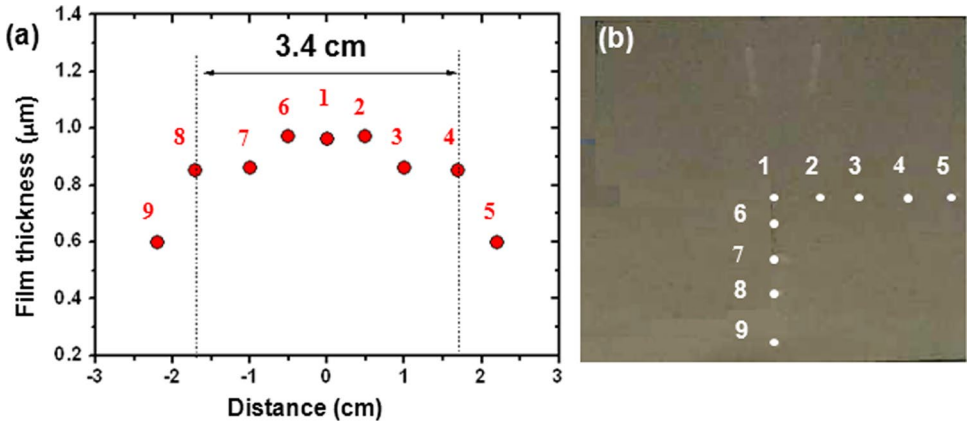

Fig. 4 **a** Thickness uniformity test performed from the center of the film along two perpendicular directions (labeled by positive and negative coordinates) for the 1-μm-thick boron coating deposited by PLD onto a Si substrate; **b** thickness measurement points over the surface of the sample under examination (labeled by positive and negative coordinates)

Turning to the PLD depositions performed onto C substrates, Fig. 6 compares the boron coatings covering a smooth C substrate (left panel) and a textured C substrate referred to as rough C substrate (right panel). On comparing with the boron film deposited onto Al under the same experimental conditions, similar surface features can be observed that, as already discussed, can be ascribed to the mechanisms of nanosecond laser ablation. The deposit onto the textured C substrate exhibits a larger density of spherical droplets with size larger than a few micrometers and a background of smaller micrometer-sized particles which are larger as compared to the case of the not textured C substrate. As discussed in regard to the case of Al substrate, the presence of micrometer droplets can be ascribed to the typical mechanisms of nanosecond laser ablation. On the other hand, under nanosecond ablation regime, nucleation and coalescence effects of small nuclei and energetic vapor species both in the expanding plume and onto the substrate, driven by the hyperthermal growth kinetics, lead to the nucleation of particles smaller than the droplet features. These considerations account for the common surface features exhibited by the deposits obtained onto untextured and textured C substrates (Fig. 6).

On comparing flat and textured C substrates, the presence of edges and wirelike features of the textured C substrate can introduce trapping zones and curvature effects that are expected to influence the mobility paths of the hyperthermal deposited species. Two kinds of mechanisms can be envisaged to explain the larger surface features in the case of the textured C substrate: first, overlapping, and subsequent coalescence, of droplets and splashing favored by shadow effects of the wirelike crossed features (yellow arrows in Fig. 6e, f); second, the Ostwald ripening mechanism, i.e., growth of larger features at the expense of the smaller ones by attachment of diffusing adatoms/clusters originating from the vaporized part of the plasma plume, favored by curvature and morphological constraints of the wirelike features. Further experiments are in progress to assess these mechanisms as a function of the deposition conditions.

The results of chemical investigation carried out by the EDS technique are reported in Fig. 7 for the boron coating deposited by PLD onto smooth C substrate (Fig. 7a–c) and rough C substrate (Fig. 7d–f). Panels (a) and (d) show the microscope image of the investigated area where the measurement points are pointed out by a cross and a numeric label. For any sample, the measurement points were chosen as associated with a microdroplet and surroundings.

Panels (b) and (e) report on the boron signal detected for each EDS measurement point. Panels (c) and (f) show the EDS spectra corresponding to the measurement points with indication of the position of the Kα peaks of B, C, N and O elements.

Notably, in the case of the investigated areas and for both samples, the boron signal acquired on the droplet is larger than the one detected for the surrounding regions, which is consistent with a larger thickness sampled by the electron beam. The EDS measurements also indicate that the distribution of boron around the droplet is uniform: comparable signals resulted from the measurement points 2 and 3 in the case of smooth C substrate and from the measurement points 2, 4, 5 and 6 in the case of rough C substrate. In addition, the EDS spectra in Fig. 7c, f depict negligible contribution from contaminants in all the EDS measurement points of both samples.

Noteworthy, by comparing the intensity of the boron signal resulting from EDS measurement performed, under the same conditions, for the boron coatings deposited by PLD onto smooth and rough C substrates in the measurement

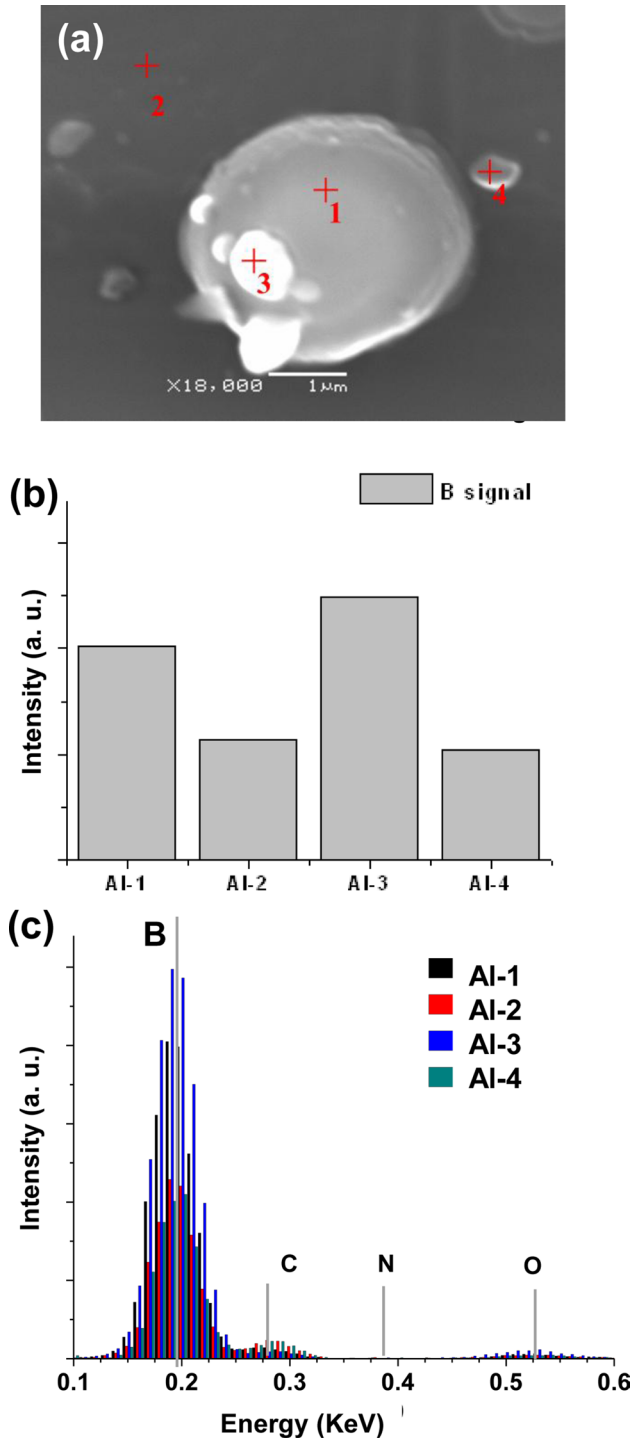

Fig. 5 EDS elemental analysis of the 1-μm-thick boron coating deposited by PLD onto a 1-mm-thick Al substrate. **a** Microscope image of the investigated area with indication of the measurement points, **b** boron signal measured over the measurement points labeled by an associated number. **c** Abundance of boron and contaminants (O, N, C) in the spot spectrum corresponding to each EDS measurement point

points detailed in Fig. 7, a systematically higher value in the case of the smooth C substrate was observed (Fig. 8). This issue can be accounted for by the fact that, under identical deposition conditions, the rough substrate offers a larger surface area over which the species of the plasma plume can distribute. All of this has to be considered while testing the efficiency performances of our boron samples as neutron converter layers.

3.2 Neutron detection performances

Although this paper mainly aims at the optimization of the deposition aspects by PLD of boron-based thick films, we also present a preliminary result about the effectiveness of the ^{10}B-enriched boron layer, deposited onto 1-mm-thick Al, as a neutron converter. For this purpose, we used the simple detector configuration described in the Experimental section and shown in Fig. 2.

The neutron detection performances obtained experimentally were compared with a GEANT4 [43] simulation of the detector irradiated with thermal neutrons. The detector geometry and materials, including the iron box, were coded in GEANT4. The simulation consisted in the irradiation of the detector with 10^6 thermal neutrons, generated on the outer box and impinging perpendicularly on the converter. An isotropic irradiation was tested as well, with no difference in the results apart from a much lower statistics.

The number of measured neutron captures, as a function of the energy deposited onto the silicon detector, is reported in Fig. 9. The large error bars are due to the poor statistics (the source activity was quite low) and to the fact that each data value is obtained by difference between the measurement with the ^{10}B facing the detector and the one with the reversed converter. On the same plot, we reported the spectrum resulting from the simulation, suitably rescaled in arbitrary units. The two structures visible in the spectrum are due to the detection of α particles (the one at higher energy) and ^{7}Li (at lower energy). At very low energy, the spectrum goes down abruptly because of a physical threshold due to the presence of the 0.2-mm-thick air layer between converter and detector and of a 500-nm-thick aluminum metallization layer on the detector surface. Based on the well-known ^{10}B(n,α)^{7}Li cross section, the maximum theoretical efficiency of a 1-μm-thick converter layer should be around 5%. The simulation tells us that, due to self absorption in the converter, the air and aluminum dead layers, and the angular distribution of the reaction products, the expected neutron detection efficiency is of the order of 2.5%. This result, along with the agreement between data and simulation in Fig. 9, is quite encouraging, and it indicates that, by means of our technology, converter layers suitable for thermal neutron detection can be produced.

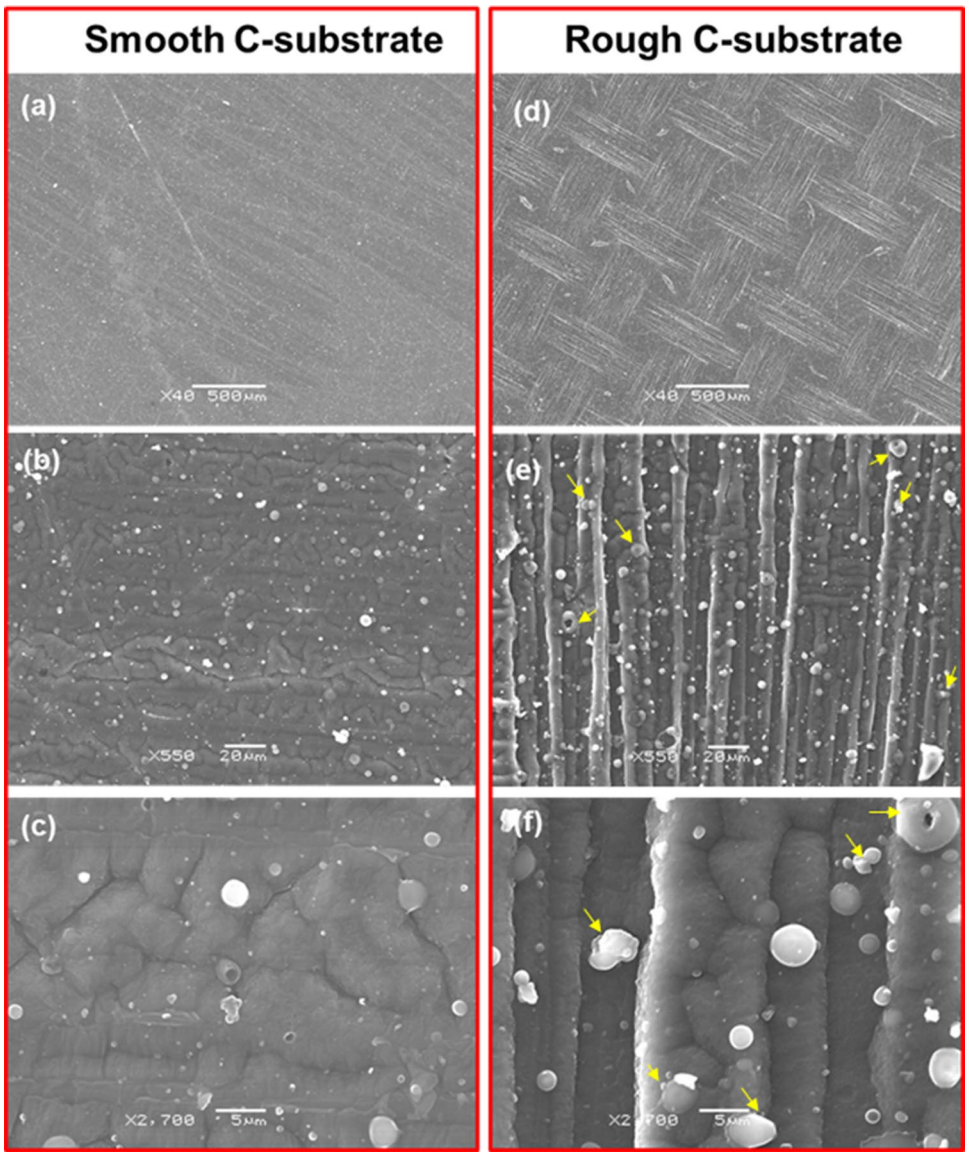

Fig. 6 SEM plan view micrographs with progressively increasing magnification of the boron coatings deposited onto **a–c** smooth C substrate and **d–f** rough (textured) C substrate

We do not present and discuss further tests performed for the boron films deposited onto smooth and textured C substrates because such results will be the subject of a future dedicated paper. For the sake of completeness, we mention that our preliminary results would indicate that the texture of the substrate has interesting consequences on the neutron detection ability of a boron converter layer.

4 Conclusions

A neutron-to-charge converter nucleus with high thermal neutron capture cross section and high-energy reaction products, such as isotope boron-10 (^{10}B), is presently widely investigated as an alternative to the expensive and decreasingly available ^{3}He nuclei in the field of solid-state neutron detectors. The fabrication of boron-based coatings is technologically challenging due to difficulties in evaporating and sputtering boron sources due to high melting point and lightweight of boron.

Among techniques applied to grow boron films, PLD is a promising method to overcoming adhesion problems, let the growth of phases difficult to deposit by other techniques and limit environmental contaminants by controlled vacuum conditions and no usage of toxic gases and solvents.

In this study, we have demonstrated the successful PLD deposition of well adherent 1-μm-thick ^{10}B-enriched boron coatings onto 1-mm-thick Al substrate as well as smooth and

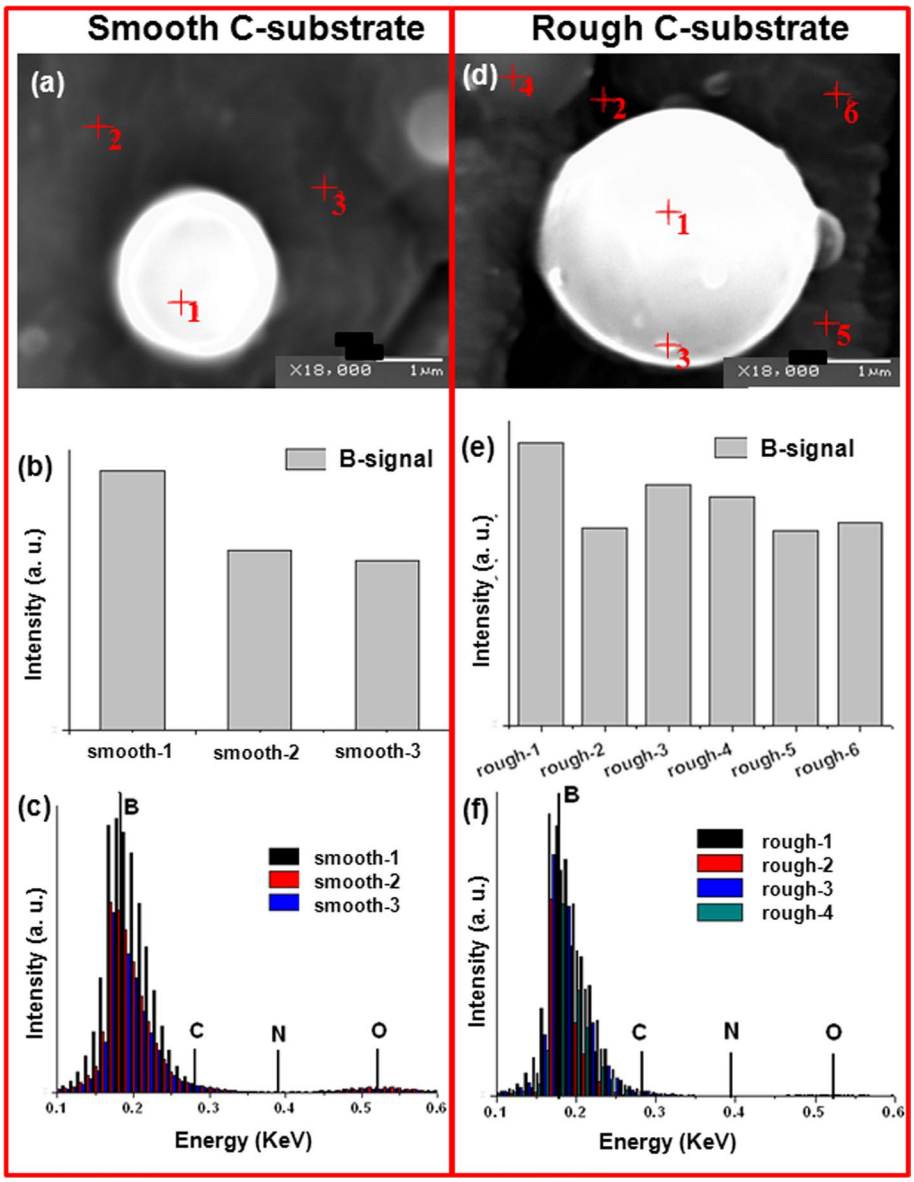

Fig. 7 EDS elemental analysis of the boron coating deposited by PLD onto **a**–**c** smooth C substrate and **d**–**f** rough C substrate. **a**, **d** show the microscope image of the investigated area with the measurement points. **b**, **e** report on the B signal corresponding to each EDS measurement point. **c**, **f** show the EDS spectra corresponding to each measurement point with indication of the energy of B and common contaminants

rough C substrates with controlled composition and thickness on a relatively large area. The first harmonic (1064 nm) of a Nd-YAG laser beam has been used under off-axis deposition geometry and high fluence (~ 10 J/cm^2) conditions.

Interplay between plasma plume divergence and peaked profile as well as target rotation has enabled to get uniform ^{10}B films over an area of a 3.4 × 3.4 cm^2.

The presented detailed investigation of morphology and elemental composition of the deposited films performed by SEM and EDS analyses has pointed out that they present the typical morphological characteristics due to the ablation mechanisms in the nanosecond regime and negligible presence of environmental contaminants, such as O, N and C, as a result of well-calibrated vacuum conditions prior to PLD depositions.

Preliminary results about the effectiveness of the ^{10}B-enriched boron layer, deposited onto 1-mm-thick Al, as a neutron converter have been presented too. Our experiments have demonstrated very encouraging performance, confirmed by simulations as well.

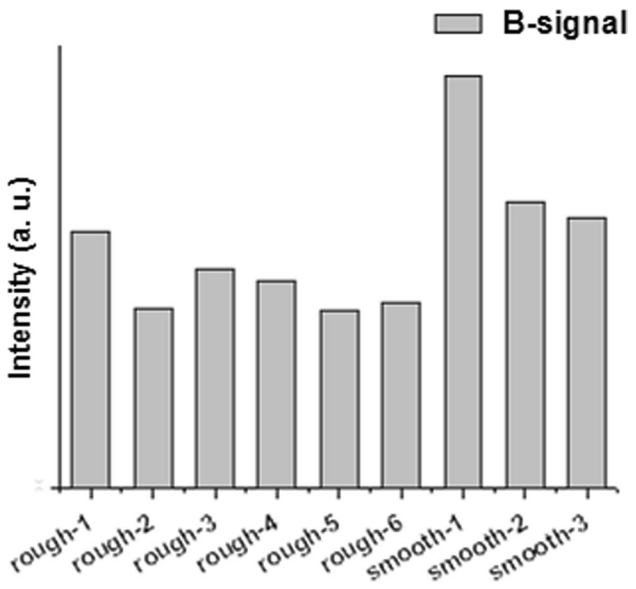

Fig. 8 Comparison between the intensity of the boron signal resulting from EDS measurement performed under the same conditions for the boron coatings deposited by PLD onto smooth and rough (textured) C substrates in the measurement points detailed in Fig. 7

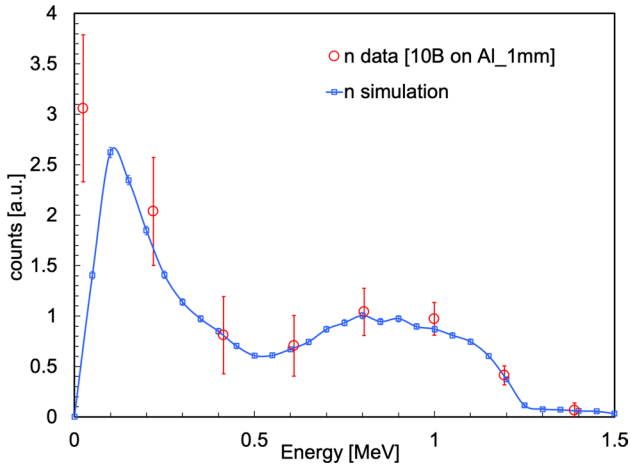

Fig. 9 Spectrum of the energy deposited by the products of neutron capture in ^{10}B. Squares: GEANT4 simulation; circles: real data. See the text for details

Acknowledgements The research activities leading to this work were supported by the National Institute of Nuclear Physics – INFN (BOLAS project).

Compliance with ethical standards

Conflict of interest The authors declare that they have no conflict of interest.

References

1. A.R. Oganov, V.L. Solozhenko, J. Superhard Mater. **31**, 285 (2009)
2. D.E. Sands, J.L. Hoard, JACS **79**, 5582 (1957)
3. P. Ball, Nat. Mater. **9**, 6 (2010)
4. A.R. Oganov, J. Chen, C. Gatti, Y. Ma, Y. Ma, C.W. Glass, Z. Liu, T. Yu, O.O. Kurakevych, V.L. Solozhenko, Nature **457**, 863 (2009)
5. G.V. Tsagareishvili, F.N. Tavadze, Prog. Cryst. Growth Charact. **16**, 341–365 (1988)
6. T. Kondo, Sci. Technol. Adv. Mater. **18**, 780 (2017)
7. Y. Tian, Z. Guo, T. Zhang, H. Lin, Z. Li, J. Chen, S. Deng, F. Liu, Nanomaterials **9**, 538 (2019)
8. Z. Zhang, E.S. Penev, B.I. Yakobson, Chem. Soc. Rev. **46**, 6746 (2017)
9. K. Kamimura, T. Yoshimura, T. Nagaoka, M. Nakao, Y. Onuma, M. Makimura, J. Solid State Chem. **154**, 153 (2000)
10. C.C. Klepper, R.C. Hazelton, E.J. Yadlowsky, E.P. Carlson, M.D. Keitz, J.M. Williams, R.A. Zuhr, D.B. Poker, J. Vac, Sci. Technol. A **20**, 725 (2002)
11. C.C. Klepper, J.M. Williams, J.J. Truhan, J. Qu, L. Riester, R.C. Hazelton, J.J. Moschella, P.J. Blau, J.P. Anderson, O.O. Popoola, M.D. Keitz, Thin Solid Films **516**, 3070 (2008)
12. M. Vidal-Dasilva, M. Fernández-Perea, J.A. Méndez, J.A. Aznárez, J.I. Larruquert, Appl. Opt. **47**, 2926 (2008)
13. T. Taylor, G. Fourlaris, P. Evans, G. Bright, Mater. Sci. Technol. **30**, 818 (2014)
14. C.C. Klepper, O.R. Monteiro, E.P. Carlson, M.D. Keitz, J. Vac. Sci. Technol. B Microelectron. Nanometer Struct. **27**, 14 (2009)
15. B. Clement, A. Bes, A. Lacoste, R. Combe, V.V. Nesvizhevsky, G. Pignol, D. Rebreyend, Y. Xi, J. Instrum. (2019). arXiv:1902.09232
16. A. Klett, Neutron detection, in *Handbook of Particle Detection and Imaging*, ed. by C. Grupen, I. Buvat (Springer, Berlin, 2019)
17. G.A. Webster, A.N. Ezeilo, Phys. B **234–236**, 949 (1997)
18. L.T. Aldrich, A.O. Nier, Phys. Rev. **74**, 1590 (1948)
19. D.A. Shea, D. Morgan, In Report No. R41419 (2010). https://fas.org/sgp/crs/misc/R41419.pdf
20. T. M. Persons, G. Aloise,GAO-11-753 (2011). https://www.gao.gov/assets/590/585514.pdf
21. M.A. Angulo, *Mineral Commodity Summaries: Boron, United States Geological Survey Minerals Yearbook* (2008). https://www.usgs.gov/centers/nmic/boron-statistics-and-information
22. M. Audronis, P.J. Kelly, A. Leyland, A. Matthews, Plasma Proc. Polym. **4**, S160 (2007)
23. F. Richter, G. Krannich, J. Hahn, R. Pintaske, M. Friedrich, S. Schmidbauer, D.R.T. Zahn, Surf. Coat. Technol. **90**, 178 (1997)
24. E. Oks, A. Anders, A. Nikolaev, Y. Yushkov, Rev. Sci. Instrum. **88**, 043506 (2017)
25. M.A. McKernan, Surf. Coat. Technol. **49**, 411 (1991)
26. H. Kodama, M. Oyaidzu, M. Sasaki, H. Kimura, Y. Morimoto, Y. Oya, M. Matsuyama, A. Sagara, N. Noda, K. Okuno, J. Nucl. Mater. **329–333**, 889 (2004)
27. L.K. Nanver, T.L.M. Scholtes, F. Sarubbi, W.B.d. Boer, G. Lorito, A. Šakic, S. Milosavljevic, C. Mok, L. Shi, S. Nihtianov, K. Buisman, in *2010 18th International Conference on Advanced Thermal Processing of Semiconductors (RTP)* (2010), pp. 136–139
28. L.B. Bayu Aji, A.A. Baker, J.H. Bae, A.M. Hiszpanski, E. Stavrou, S.K. McCall, S.O. Kucheyev, Appl. Surf. Sci. **448**, 498 (2018)
29. K. Kamimura, M. Ohkubo, T. Shinomiya, M. Nakao, Y. Onuma, J. Solid State Chem. **133**, 100 (1997)
30. S. Komatsu, Y. Moriyoshi, J. Cryst. Growth **89**, 560 (1988)
31. M. Oyaidzu, A. Yoshikawa, H. Kodama, Y. Oya, A. Sagara, N. Noda, K. Okuno, Appl. Surf. Sci. **244**, 240 (2005)

32. A. Matthews, K.S. Fancey, A.S. James, A. Leyland, Surf. Coat. Technol. **61**, 121 (1993)
33. D. Dellasega, V. Russo, A. Pezzoli, C. Conti, N. Lecis, E. Besozzi, M. Beghi, C.E. Bottani, M. Passoni, Mater. Des. **134**, 35 (2017)
34. T. Moscicki, Int. J. Opt. **2016**, 13 (2016)
35. Z.-F. Song, S.-Z. Ye, Z.-Y. Chen, L. Song, J. Shen, Appl. Radiat. Isot. **69**, 443 (2011)
36. Z. Wang, Y. Shimizu, T. Sasaki, K. Kirihara, K. Kawaguchi, K. Kimura, N. Koshizaki, J. Solid State Chem. **177**, 1639 (2004)
37. A.P. Caricato, G. Quarta, D. Manno, M. Cesaria, A. Perrone, M. Martino, A. Serra, L. Calcagnile, G. Barone, A. Lorusso, Appl. Surf. Sci. **483**, 1044 (2019)
38. R.K. Singh, J. Narayan, Phys. Rev. B **41**, 8843 (1990)
39. M. Cesaria in *Surface Energy and Nucleation Modes, in Pulsed Laser Ablation: Advances and Applications in Nanoparticles and Nanostructuring* ed. by I.N. Mihailescu, A.P. Caricato (Pan Stanford Publishing Pte Ltd 2018)
40. M. Siegert, W. Zander, J. Lisoni, J. Schubert, C. Buchal, Appl. Phys. A **69**, S779 (1999)
41. J.H. Yoo, S.H. Jeong, X.L. Mao, R. Greif, R.E. Russo, Appl. Phys. Lett. **76**, 783 (2000)
42. J. Hoffman, J. Phys. D Appl. Phys. **48**, 235201 (2015)
43. S. Agostinelli, J. Allison, K. Amako, J. Apostolakis, H. Araujo, P. Arce, M. Asai, D. Axen, S. Banerjee, G. Barrand, F. Behner, L. Bellagamba, J. Boudreau, L. Broglia, A. Brunengo, H. Burkhardt, S. Chauvie, J. Chuma, R. Chytracek, G. Cooperman, G. Cosmo, P. Degtyarenko, A. Dell'Acqua, G. Depaola, D. Dietrich, R. Enami, A. Feliciello, C. Ferguson, H. Fesefeldt, G. Folger, F. Foppiano, A. Forti, S. Garelli, S. Giani, R. Giannitrapani, D. Gibin, J.J. Gómez Cadenas, I. González, G. Gracia Abril, G. Greeniaus, W. Greiner, V. Grichine, A. Grossheim, S. Guatelli, P. Gumplinger, R. Hamatsu, K. Hashimoto, H. Hasui, A. Heikkinen, A. Howard, V. Ivanchenko, A. Johnson, F.W. Jones, J. Kallenbach, N. Kanaya, M. Kawabata, Y. Kawabata, M. Kawaguti, S. Kelner, P. Kent, A. Kimura, T. Kodama, R. Kokoulin, M. Kossov, H. Kurashige, E. Lamanna, T. Lampén, V. Lara, V. Lefebure, F. Lei, M. Liendl, W. Lockman, F. Longo, S. Magni, M. Maire, E. Medernach, K. Minamimoto, P. Mora de Freitas, Y. Morita, K. Murakami, M. Nagamatu, R. Nartallo, P. Nieminen, T. Nishimura, K. Ohtsubo, M. Okamura, S. O'Neale, Y. Oohata, K. Paech, J. Perl, A. Pfeiffer, M.G. Pia, F. Ranjard, A. Rybin, S. Sadilov, E. Di Salvo, G. Santin, T. Sasaki, N. Savvas, Y. Sawada, S. Scherer, S. Sei, V. Sirotenko, D. Smith, N. Starkov, H. Stoecker, J. Sulkimo, M. Takahata, S. Tanaka, E. Tcherniaev, E. Safai Tehrani, M. Tropeano, P. Truscott, H. Uno, L. Urban, P. Urban, M. Verderi, A. Walkden, W. Wander, H. Weber, J.P. Wellisch, T. Wenaus, D.C. Williams, D. Wright, T. Yamada, H. Yoshida, D. Zschiesche, Nucl. Instrum. Methods Phys. Res. Sect. A Accel. Spectrom. Detect. Assoc. **506**, 250 (2003)